Article

Chassis Influence on the Exposure Assessment of a Compact EV during WPT Recharging Operations

Valerio De Santis [1,*], Luca Giaccone [2], and Fabio Freschi [2]

[1] Department of Industrial and Information Engineering and Economics, University of L'Aquila, L'Aquila, Italy; valerio.desantis@univaq.it
[2] Dipartimento Energia "G. Ferraris", Politecnico di Torino, corso Duca degli Abruzzi, 24, Torino, Italy; luca.giaccone@polito.it; fabio.freschi@polito.it
* Correspondence: valerio.desantis@univaq.it

Abstract: In this study, the external magnetic field emitted by a wireless power transfer (WPT) system and the internal electric field induced into human body models during recharging operations of a compact electric vehicle (EV) are evaluated. To this aim an ad-hoc formulation for the source modeling is coupled with a commercial software that performs numerical dosimetry. Specifically, two realistic anatomical models both in a driving position and in a standing posture are considered, and the chassis of the EV is modeled either as a currently employed aluminum alloys and as a futuristic carbon fiber composite panel. Aligned and misaligned coil configurations of the WPT system are considered as well. The analysis of the obtained results shows that the ICNIRP reference levels are exceeded in the driving position, especially for the carbon fiber chassis, whereas no exceedance is observed in terms of basic restrictions, at least for the considered scenarios.

Keywords: Computational electromagnetics; Electric Vehicle; EMF safety; low frequency dosimetry; Wireless Power Transfer

1. Introduction

The air quality is becoming a health problem in many cities around the world. This is mainly due to the transportation sector, which is one of the main contributors towards global climate change and CO_2 emissions [1]. Thus, the usage of compact electric vehicles (EVs), together with the development of new mobility services, are the most sustainable solution for the city. However, despite their interest, EV deployment on a global scale is still hampered by the battery technology and charging infrastructure [2]. These drawbacks can be resolved through static or dynamic wireless power transfer (WPT) systems and their widespread applications in an improved charging infrastructure for EVs [3].

One more challenge pertinent with compact EVs is related to the choice of the chassis materials. Indeed, small EVs have to combine both mechanical strength, since they are seen as unsafe vehicles by most of the users, and lightweight to extend battery life or increase vehicle performances. Current materials employed for the car body are aluminum (Al) alloys, but in the future advanced lightweight materials, such as carbon fiber (CF) composite panels, could be widely used [4]. If on one hand the latter can reduce the weight and the emission of the vehicles, on the other hand the reduced conductivities of CF materials, which yields to lower shielding capabilities, arise more concerns about the EMF safety of passengers and bystanders.

This paper therefore deals with the evaluation of the human exposure to the magnetic field emitted by a WPT system aimed to recharge the battery of a compact car, namely a FIAT 500, when both Al and CF chassis are considered. The standalone design of the recharging system, which is a stationary WPT system operating at 85 kHz, can be easily performed with classical approaches, such as finite elements. However, when dealing with human exposure, the influence of the car body and the human body must also be taken

into account [5–8]. It is well known that, within the low frequency (LF) range, the presence of the human body does not affect the source field. Therefore, it is possible to separate the complete analysis in two steps [9,10]: 1) simulation of the magnetic field source (WPT + car body) and 2) numerical dosimetry (human body subject to the previously evaluated LF field).

The study of the magnetic field source is complicated by the presence of the car body that is a large 3D surface with a very small thickness. To this aim we propose a hybrid approach based on boundary element method (BEM) and surface impedance boundary conditions (SIBCs) [11].

Numerical dosimetry in the LF frequency range is commonly performed using the scalar potential finite difference (SPFD) formulation [9]. In this paper, the commercial software Sim4Life (`https://zmt.swiss/sim4life`) has been employed. It makes use of the magnetic vector potential at the right hand side that is not readily accessible from the hybrid formulation described earlier. For this reason a curl-inversion procedure is used to compute a compatible magnetic vector potential starting from the magnetic flux density [12–14]. Sim4Life implemented this procedure on the base of a previous work of the authors [12].

2. Materials and Methods

2.1. Car modeling

The compact vehicle considered in this paper is the well-known FIAT 500 Italian car. A model suitable for electromagnetic computations is not so easy to be identified. To give an example, the commercial CAD available at `https://hum3d.com/3d-models/fiat-500` includes many details such as the license plate, some internal components, the logo of the CAD provider, that make the generation of a good mesh very hard (see Figure 1(a)). For this reason, a brand new CAD has been developed keeping in mind that it had to be used for numerical electromagnetic simulations (see Figure 1(b)). By using the following link `https://github.com/cadema-PoliTO/vehicle4em`, the hereby considered, together with other CAD models of vehicles, can be freely obtained.

In this paper, only the chassis of the car has been considered and modeled as a surface mesh (see Figure 1(c)), since the numerical formulation is based on the SIBC method [11]. Indeed, at such frequencies, the geometrical thickness (i.e., about 2 cm) is usually much larger than the electrical skin depth of the chassis material. In order to investigate the effect of the car body shielding on the exposure assessment, two different materials have been considered: aluminum and carbon fiber. The former represents current adopted material in compact vehicles, while the latter could be employed in future EVs. A conductivity of $\sigma = 3 \times 10^7$ S/m has been used for the aluminum, whereas a homogeneous conductivity of $\sigma = 4 \times 10^4$ S/m was employed for the CF, as derived in [15].

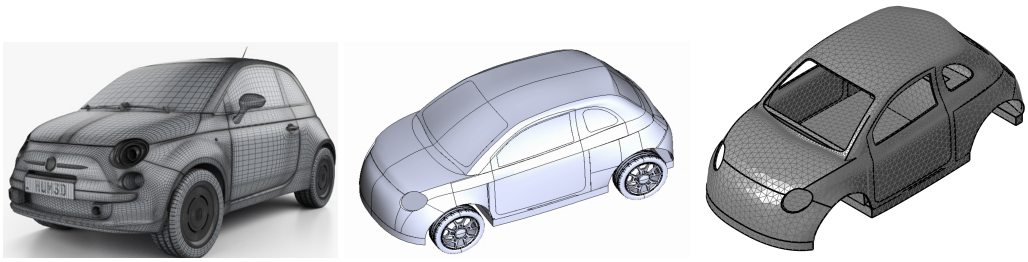

(a) **(b)** **(c)**

Figure 1. Commercial CAD model of a FIAT 500 **(a)**, simplified CAD model for electromagnetic simulations **(b)**, surface mesh used in this paper **(c)**.

2.2. WPT system configuration

Recently, several standards for WPT applications in EVs have been established. Among these, the International Electrotechnical Commission (IEC) and the Society of Automotive Engineers (SAE) are the most adopted [16,17]. They mainly specify the transfer power and the operational frequency of the WPT system, together with other parameters and specifications. For a compact size car, as the considered one, the transfer power is set to 7.7 kVA, while the operational frequency is fixed to 85 kHz.

The WPT system considered in this study is the WPT2/Z3 configuration described in the Recommended Practice SAE J2954 [17]. Specifically, each coil is made of 8 turns and the current flowing into a single-turn is 26 A for the transmitter and j26 A for the receiver. Both coils are shielded by two thin-layers of aluminum and ferrite with an outer dimension of approximately 420×420 mm^2, as shown in Figure 2.

In order to investigate the worst exposure scenario, both the case of perfect alignment (see Figure 2(a) and Figure 2(b)) and of maximum misalignment, as suggested by SAE J2954 [17], i.e., $d_x = -75$ mm and $d_y = 100$ mm (see Figure 2(c) and Figure 2(d)), have been considered.

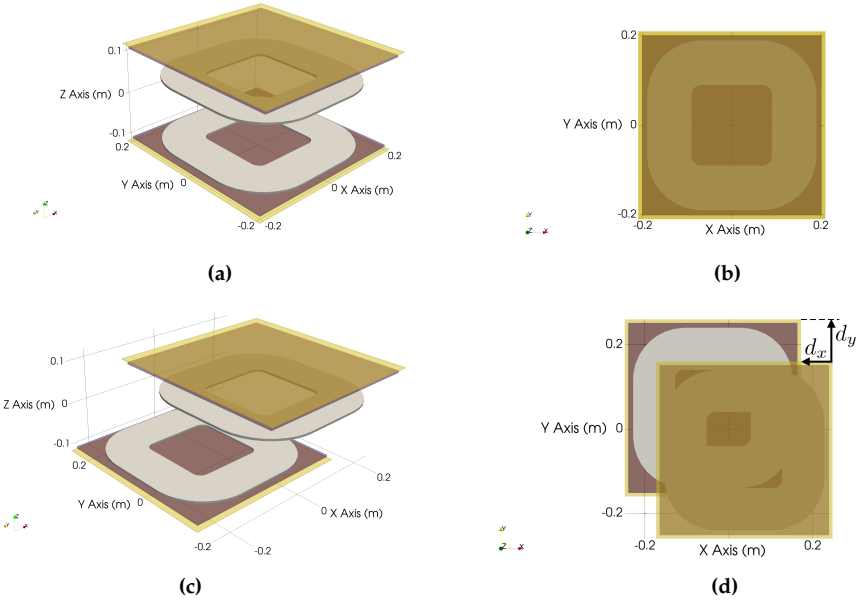

Figure 2. WPT2/Z3 system with perfect alignment **(a)-(b)** and maximum misalignment **(c)-(d)**.

2.3. Exposure scenarios for numerical dosimetry

The exposure scenarios consist of two realistic anatomical models placed nearby or inside the car, as illustrated in Figure 3. Specifically, Duke and Ella from the Virtual Population ViP 3.0 (`https://itis.swiss/virtual-population`) have been employed. The former is in a driving position at a distance $t_z = 30$ cm from the secondary coil, while the latter is in a standing posture outside the car at a distance $t_y = 22.3$ cm from the primary coil in the misaligned position (see Figure 3(b)).

Tissue dielectric properties have been assigned from the IT'IS database [18], with the exception of the skin where a higher conductivity value has been adopted, as described in [19,20].

2.4. Magnetic field evaluation

The magnetic field source coming from the WPT system and shielded by the car body is modeled using an hybrid formulation [11]. It is evaluated inside the box regions embedding the anatomical models (see Figure 3(a)), which are not considered in this stage since they do not perturb the magnetic field at such frequencies [21]. In this paper we make

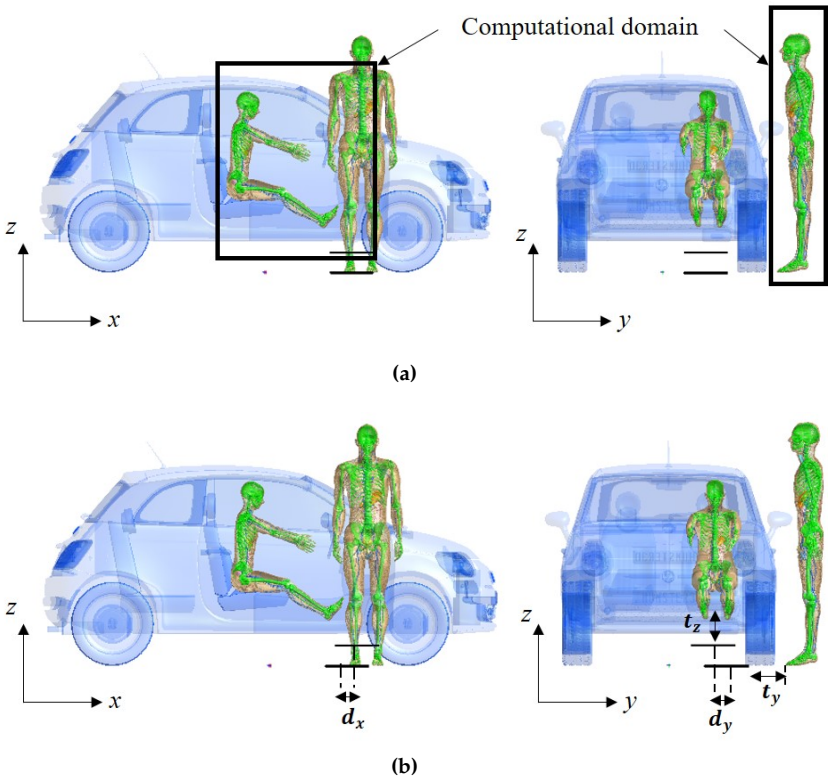

Figure 3. Exposure scenarios for the aligned **(a)** and misaligned **(b)** coils.

use of the algebraic framework [22]. BEM equations, topological equations, constitutive equations and continuity equations are coupled to obtain the final system:

$$\begin{bmatrix} -\mathbf{H} & \mathbf{W} \\ \mathbf{C}\mathbf{Z}\mathbf{C}^{\mathrm{T}} & \mathrm{j}\omega\mu_0\mathbf{S} \end{bmatrix} \begin{bmatrix} \boldsymbol{\psi} \\ \partial_n\boldsymbol{\psi} \end{bmatrix} = \begin{bmatrix} \mathbf{0} \\ \mathbf{b} \end{bmatrix} \tag{1}$$

being μ_0 the permeability of the air, ω the angular frequency, $\mathbf{H}$ and $\mathbf{W}$ the standard matrices of the BEM formulation, $\boldsymbol{\psi}$ and $\partial_n\boldsymbol{\psi}$ the reduced magnetic scalar potential and its normal derivative, $\mathbf{Z}$ the impedance matrix that links current to voltages, $\mathbf{S}$ the matrix with triangle surfaces and $\mathbf{C}$ is the discrete curl operator. The right hand side is defined as $\mathbf{b} = \mathbf{C}\mathbf{Z}\mathbf{h}_{\mathrm{S}} + \mathrm{j}\omega\mu_0\mathbf{S}\mathbf{H}_{\mathrm{S}n}$, where, $\mathbf{h}_{\mathrm{S}}$ is magnetic field created by the source currents on the primal edges and $\mathbf{H}_{\mathrm{S}n}$ is the orthogonal components of the same magnetic field on the triangles.

For naïve problems, direct solvers can be used to solve (1). However this approach becomes impractical for medium scale problems, because the lower-left block requires the preliminary calculation of the impedance matrix $\mathbf{Z} = \mathbf{Y}^{-1}$. The explicit inversion of the admittance matrix is computationally intensive and gives rise to a dense block in addition to the BEM matrices $\mathbf{H}$ and $\mathbf{W}$ [11].

For nontrivial problems, the complex nonsymmetric indefinite system is solved by an iterative Krylov-subspace solver like GMRES [23]. With the use of iterative solvers, the effective availability of the matrix in (1) is not strictly necessary, but only the matrix vector product is required. To this aim the effective calculation of $\mathbf{Z}$ can be avoided in favor of a more efficient LU factorization.

As suggested in [24], the spectral properties of (1) can be further improved by calculating the Schur complement of the lower-right block $\mathrm{j}\omega\mu_0\mathbf{S}$, and solving with respect to $\partial_n\boldsymbol{\psi}$:

$$\partial_n\boldsymbol{\psi} = -\mathbf{H}_{Sn} + (\mathrm{j}\omega\mu_0\mathbf{S})^{-1}\left(\mathbf{C}\mathbf{Z}\mathbf{C}^{T}\boldsymbol{\psi} - \mathbf{C}\mathbf{Z}\mathbf{h}_{S}\right) \tag{2}$$

Substituting (2) in (1) it yields:

$$\left[\mathbf{H} + \mathbf{W}(\mathrm{j}\omega\mu_0\mathbf{S})^{-1}\mathbf{C}\mathbf{Z}\mathbf{C}^{\mathrm{T}}\right]\boldsymbol{\psi} = \mathbf{b}_{\mathrm{s}} \tag{3}$$

being $\mathbf{b}_{\mathrm{s}} = \mathbf{W}(\mathrm{j}\omega\mu_0\mathbf{S})^{-1}\mathbf{C}\mathbf{Z}\mathbf{h}_{\mathrm{S}} + \mathbf{W}\mathbf{H}_{\mathrm{S}n}$.

Because the matrix $\mathbf{S}$ is diagonal, the calculation of the Schur complement is not computationally intensive. Again, the use of GMRES does not require the effective assembling of $\mathbf{H} + \mathbf{W}(\mathrm{j}\omega\mu_0\mathbf{S})^{-1}\mathbf{C}\mathbf{Z}\mathbf{C}^{\mathrm{T}}$ but only the supply of the matrix-vector product $\mathbf{H}\boldsymbol{\psi} + \mathbf{W}(\mathrm{j}\omega\mu_0\mathbf{S})^{-1}\mathbf{C}\mathbf{Z}\mathbf{C}^{\mathrm{T}}\boldsymbol{\psi}$ to the solver.

2.5. LF dosimetry

When considering LF dosimetry, the SPFD method is often the preferred one because the induced currents in the human body do not modify the source field and the problem can be formulated with the scalar potential as nodal unknowns [9]. Using the algebraic framework, the SPFD is given by [13]:

$$\mathbf{G}^{\mathrm{T}}\mathbf{M}_{\sigma}\mathbf{G}\boldsymbol{\varphi} = -\mathrm{j}\omega\mathbf{G}^{\mathrm{T}}\mathbf{M}_{\sigma}\mathbf{a}_{\mathrm{s}} \tag{4}$$

where, for a voxel-based human model, $\mathbf{M}_{\sigma}$ is a diagonal conductance matrix, $\mathbf{G}$ is the edge-to-node incidence matrix, $\mathbf{a}_{\mathrm{s}}$ is the line integral of the magnetic vector potential ($\mathbf{A}$-field) due to the sources and $\boldsymbol{\varphi}$ is the electric scalar potential [13].

The magnetic vector potential is not readily accessible from the hybrid formulation. This issue can be solved by using a curl-inversion procedure, which has extensively been described in [12–14]. In this paper we tested the commercial software Sim4Life that implemented the curl-inversion procedure based on a previous work of the authors [12]. For the sake of completeness, the equations for the curl inversion are given:

$$\begin{aligned}
A_x = & -\int_0^y \left(\frac{1}{3}B_z(x,y',z) + \frac{1}{6}B_z(x,y',0)\right)dy' \\
& +\int_0^z \left(\frac{1}{3}B_y(x,y,z') + \frac{1}{6}B_y(x,0,z')\right)dz' \\
A_y = & -\int_0^z \left(\frac{1}{3}B_x(x,y,z') + \frac{1}{6}B_x(0,y,z')\right)dz' \\
& +\int_0^x \left(\frac{1}{3}B_z(x',y,z) + \frac{1}{6}B_z(x',y,0)\right)dx' \\
A_z = & -\int_0^x \left(\frac{1}{3}B_y(x',y,z) + \frac{1}{6}B_y(x',0,z)\right)dx' \\
& +\int_0^y \left(\frac{1}{3}B_x(x,y',z) + \frac{1}{6}B_x(0,y',z)\right)dy'
\end{aligned} \tag{5}$$

With reference to Figure 4, the numerical model of the source is used to compute the $\mathbf{B}$-field at discrete points in a bounded hexahedral grid and Equation (5) is then used to get the $\mathbf{A}$-field at the same points. This $\mathbf{A}$-field distribution is interpolated on the human model and eventually the electric scalar potential is obtained by solving Equation (4). It is worth stressing that Figure 4 is purely descriptive and more points have been used in actual simulations. The relative error introduced in the solution is shown to be negligible for a discretization of the bounded volume in the order of centimeters [14]. Finally, by knowing the electric scalar potential $\boldsymbol{\varphi}$, it is straightforward to compute the induced electric field in the human body as required by the dosimetric assessment.

3. Numerical dosimetry results

The exposure assessment of the investigated WPT system against the EMF limits provided by the International Commission on Non-Ionizing Radiation Protection (ICNIRP) is hereby provided [25]. First, compliance against the reference level (RL), i.e., the magnetic field computed outside or inside the car body is determined without the presence of the

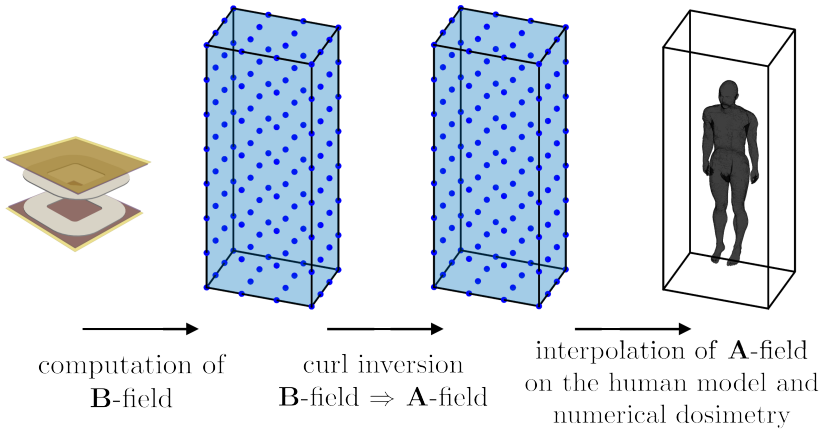

Figure 4. The human model is bounded in a hexahedral grid. Knowing the **B**-field at the blue points it is possible to define a compatible **A**-field that, after interpolation, is used as source term in (4).

exposed human models. Then, the basic restriction (BR), i.e., the electric field induced inside the human body is evaluated.

3.1. RL numerical dosimetry

Figure 5(a) and Figure 5(b) depict the magnetic field distributions inside the computational domain when considering an Al chassis for both aligned and misaligned coil configurations, respectively. The same is reported in Figure 6(a) and Figure 6(b) for the CF chassis. In these figures, the anatomical models are overlaid to the exposure scenario for the only sake of clarity, i.e., to facilitate the compliance. Indeed, the green areas are the region where the RL (i.e., $B_{lim} = 27\ \mu$T) is exceeded. As can be observed, the ICNIRP-RL is never exceeded in Duke standing outside for both chassis materials (almost exceeding for the misaligned case). Instead, it is barely exceeded in the heel of Ella driving in the car body made of aluminum, while it is largely exceeded in the leg and feet areas for the CF chassis. Thus, compliance against BR is needed in these latter cases.

3.2. BR numerical dosimetry

The induced electric field distributions inside the two anatomical models are reported in Figure 7 for both chassis materials and both coil positions, respectively. The obtained results show that the ICNIRP-BR is exceeded only in a small portion of the feet for the driving passenger in the CF chassis, while no exceedance it is observed for the Al chassis and the standing person outside the car. However, it is worth noting that ICNIRP suggests to determine compliance against a $2 \times 2 \times 2$ mm^3 volume averaging and the 99-th percentile of the peak induced electric field [25]. In this paper we use anatomical models with a voxel resolution of 2 mm that corresponds to the averaging volume proposed by the ICNIRP, therefore only the 99-th percentile has to be computed.

To better quantify these results, the values of the exposure assessment are summarized in Table 1, where E_{max} is the peak induced electric field, whereas E_{99} is the 99-th percentile. As it can be observed, when comparing the latter with the BR, the overexposure is always negative (at least -16 dB), meaning that the considered exposure scenario is far away from exceeding the ICNIRP-BR. The Influence of the chassis material is also evident, with an average shielding of $3 - 4$ dB on the induced electric fields for the Al compared to the CF.

4. Conclusions

In this paper, the human exposure to a WPT system aimed to recharge a compact vehicle was carried out. The analysis was performed selecting suitable and separate tools to analyze the magnetic field source and to evaluate the induced electric fields. The magnetic field source was handled by an ad-hoc software based on a hybrid scheme, whereas

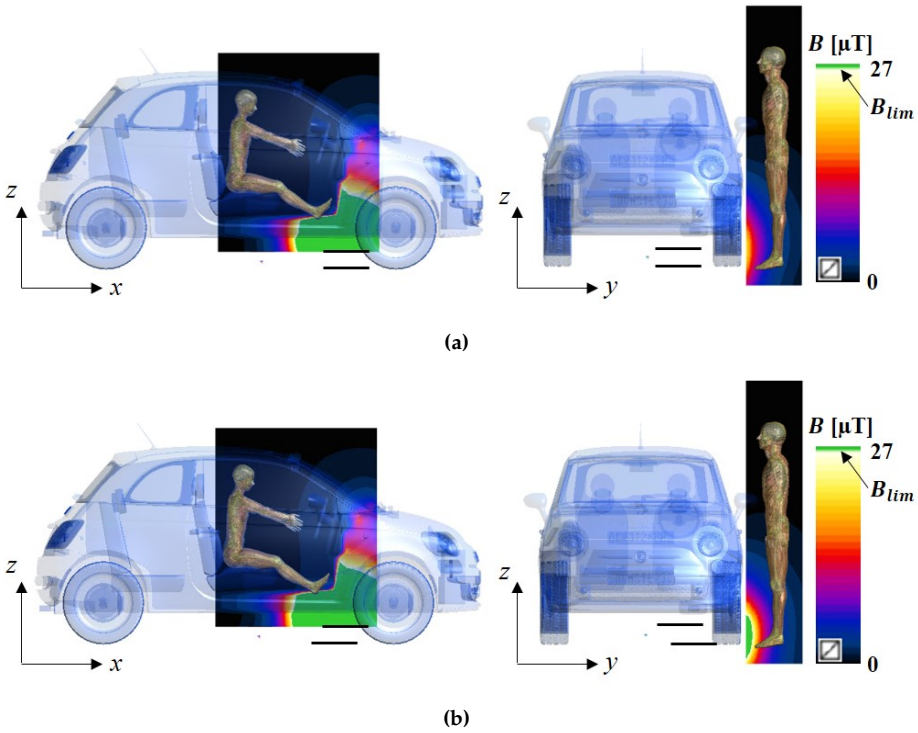

Figure 5. **B**-field distributions for the aligned **(a)** and misaligned **(b)** coil positions with the Al chassis.

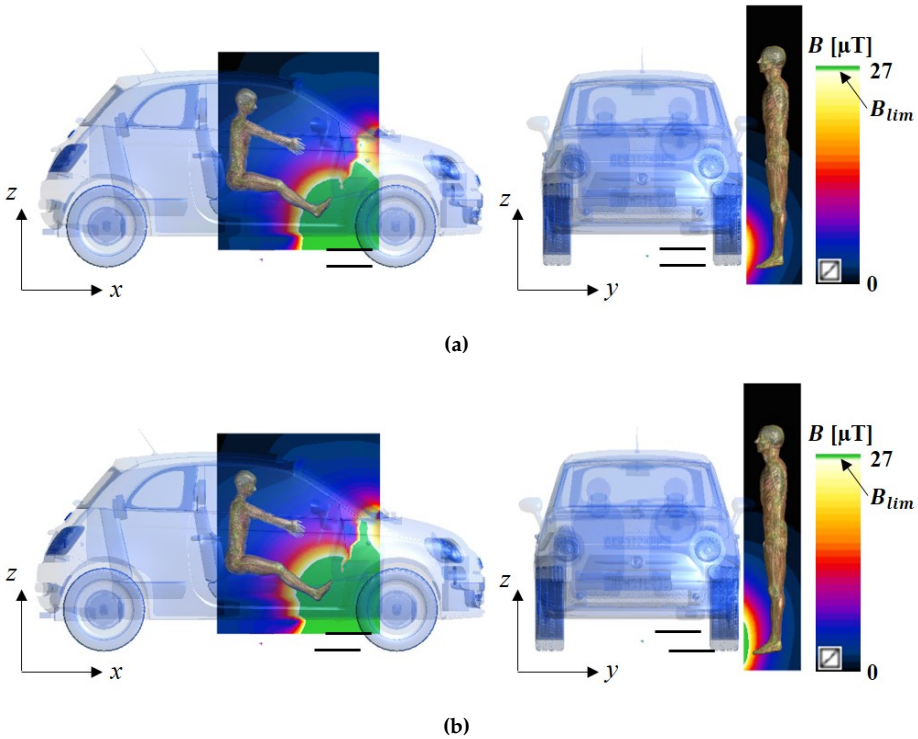

Figure 6. **B**-field distributions for the aligned **(a)** and misaligned **(b)** coil positions with the CF chassis.

the numerical dosimetry was carried out using a commercial software. The proposed formulation was able to handle the complex shape of the compact vehicle (namely a FIAT 500) in a seamless way.

In order to investigate the effect of the car body shielding on the exposure assessment, two different materials have been considered for the vehicle chassis: aluminum and carbon

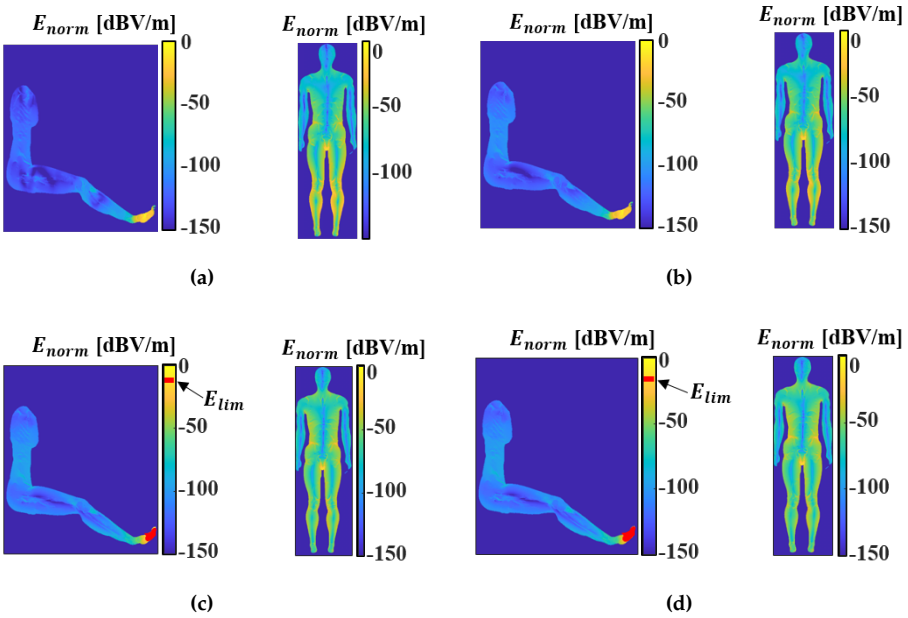

Figure 7. Induced electric field distributions inside Ella (left) and Duke (right) for the aligned **(a)** and misaligned **(b)** coil positions in the Al chassis and for the aligned **(c)** and misaligned **(d)** coil positions in the CF chassis. E_{norm} is the electric field normalized to the peak value. E_{lim} is the BR = 11.48 V/m (red area is the portion where the BR is exceeded).

Table 1. Summary of the compliance assessment with the BR for the considered exposure scenarios.

Exposure scenario	Chassis material	$E_{\max}$ (V/m)	E_{99} (V/m)	Overexposure (dB)
Ella–Aligned	aluminum	8.26	0.71	-18.48
Ella–Misaligned		7.69	0.57	-19.22
Duke–Aligned		0.27	0.07	-44.11
Duke–Misaligned		0.53	0.12	-39.56
Ella–Aligned	carbon fiber	19.21	1.71	-16.48
Ella–Misaligned		24.00	1.76	-16.23
Duke–Aligned		0.76	0.14	-38.11
Duke–Misaligned		0.90	0.17	-36.45

fiber. The former represents current adopted material in compact vehicles, while the latter should be employed more often in future EVs. Although hybrid solutions could most likely be used, these two materials therefore cover the upper- and lower-band of conductivity values that an EV cabin can assume.

The proposed method was tested on the case of a WPT system mounted close to the left front wheel. The exposure was evaluated both for the driver and a bystander. Aligned and misaligned coil configurations of the WPT system were considered as well. From the obtained results it has been shown that the considered cases are not compliant with the reference level, especially for the driver position within a car body frame made of carbon fiber. Instead, numerical dosimetry confirmed that the basic restriction is never exceeded, at least for the considered scenarios.

Author Contributions: The authors contributed equally to this work.

Funding: This research received no external funding.

Acknowledgments: Authors would like to thank Donato Manesi (Politecnico di Torino) fot the support given in the CAD modeling and Francesco Di Blasio, Gabriella Febbo (University of L'Aquila) for their valuable support with the dosimetric simulations.

Conflicts of Interest: The authors declare no conflict of interest.

References

1. International Energy Agency (IEA). Global energy and CO_2 status report, 2018.
2. International Energy Agency (IEA). Global EV outlook, 2019.
3. Machura, P.; De Santis, V.; Li, Q. Driving Range of Electric Vehicles Charged by Wireless Power Transfer. *IEEE Trans. Veh. Technol.* **2020**, *69*, 5968–5982. doi:10.1109/TVT.2020.2984386.
4. Romo, J.; Cañibano, E.; Merino, J.C. Lightweighting and passive safety for urban electric vehicle. 2017 Electric Vehicles International Conference (EV), 2017, pp. 1–5. doi:10.1109/EV.2017.8242113.
5. Shimamoto, T.; Laakso, I.; Hirata, A. In-situ electric field in human body model in different postures for wireless power transfer system in an electrical vehicle. *Phys. Med. Biol.* **2015**, *60*, 163–173. cited By 35, doi:10.1088/0031-9155/60/1/163.
6. Cirimele, V.; Freschi, F.; Giaccone, L.; Pichon, L.; Repetto, M. Human Exposure Assessment in Dynamic Inductive Power Transfer for Automotive Applications. *IEEE Trans. Magn.* **2017**, *53*, 1–4. doi:10.1109/TMAG.2017.2658955.
7. De Santis, V.; Campi, T.; Cruciani, S.; Laakso, I.; Feliziani, M. Assessment of the Induced Electric Fields in a Carbon-Fiber Electrical Vehicle Equipped with a Wireless Power Transfer System. *Energies* **2018**, *11*. doi:10.3390/en11030684.
8. Arduino, A.; Bottauscio, O.; Chiampi, M.; Giaccone, L.; Liorni, I.; Kuster, N.; Zilberti, L.; Zucca, M. Accuracy Assessment of Numerical Dosimetry for the Evaluation of Human Exposure to Electric Vehicle Inductive Charging Systems. *IEEE Trans. Electromag. Compat.* **2020**, *62*, 1939–1950. doi:10.1109/TEMC.2019.2954111.
9. Dawson, T.; Stuchly, M. Analytic validation of a three-dimensional scalar-potential finite-difference code for low-frequency magnetic induction. *Appl. Comput. Electrom.* **1996**, *11*, 72–81.
10. Zang, M.; Cimala, C.; Clemens, M.; Dutiné, J.; Timm, T.; Schmuelling, B. A Co-Simulation Scalar-Potential Finite Difference Method for the Numerical Analysis of Human Exposure to Magneto-Quasi-Static Fields. *IEEE Trans. Magn.* **2017**, *53*, 7202804/1–7202804/4.
11. Freschi, F.; Giaccone, L.; Repetto, M. Algebraic formulation of nonlinear surface impedance boundary condition coupled with BEM for unstructured meshes. *Eng. Anal. Bound. Elem.* **2018**, *88*, 104–114. doi:10.1016/j.enganabound.2017.12.008.
12. Laakso, I.; De Santis, V.; Cruciani, S.; Campi, T.; Feliziani, M. Modelling of induced electric fields based on incompletely known magnetic fields. *Phys. Med. Biol.* **2017**, *62*, 6567.
13. Freschi, F.; Giaccone, L.; Cirimele, V.; Canova, A. Numerical assessment of low-frequency dosimetry from sampled magnetic fields. *Phys. Med. Biol.* **2018**, *63*, 015029.
14. Conchin Gubernati, A.; Freschi, F.; Giaccone, L.; Campi, T.; De Santis, V.; Laakso, I. Comparison of numerical techniques for the evaluation of human exposure from measurement data. *IEEE Trans. Magn.* **2019**, *55*, 1–4. doi:10.1109/TMAG.2019.2896720.
15. Campi, T.; Cruciani, S.; De Santis, V.; Maradei, F.; Feliziani, M. Magnetic field behavior in a carbon-fiber electrical vehicle charged by a wireless power transfer system. 2017 International Symposium on Electromagnetic Compatibility - EMC EUROPE, 2017, pp. 1–6. doi:10.1109/EMCEurope.2017.8094723.
16. IEC 61980-1. Electric vehicle wireless power transfer (WPT) systems - Part 1: General requirements, 2015.
17. International SAE J2954 - Wireless Power Transfer for Light-Duty Plug-In/Electric Vehicles and Alignment Methodology, 2019.
18. Hasgall, P.A.; Di Gennaro, F.; Baumgartner, C.; Neufeld, E.; Lloyd, B.; Gosselin, M.; Payne, D.; Klingenböck, A.; Kuster, N. IT'IS Database for thermal and electromagnetic parameters of biological tissues. www.itis.swiss/database, 2018.
19. De Santis, V.; Chen, X.L.; Laakso, I.; Hirata, A. An equivalent skin conductivity model for low-frequency magnetic field dosimetry. *Biomed. Phys. Eng. Express* **2015**, *1*, 1–10. doi:10.1088/2057-1976/1/1/015201.
20. De Santis, V.; Chen, X.L.; Cruciani, S.; Campi, T.; Feliziani, M. A novel homogenization procedure to model the skin layers in LF numerical dosimetry. *Phys. Med. Biol.* **2016**, *61*, 4402–4411. doi:10.1088/0031-9155/61/12/4402.
21. Hirata, A.; Ito, F.; Laakso, I. Confirmation of quasi-static approximation in SAR evaluation for a wireless power transfer system. *Phys. Med. Biol.* **2013**, *58*, N241–N249. doi:10.1088/0031-9155/58/17/N241.
22. Tonti, E. A Direct Discrete Formulation of Field Laws: The Cell Method. *Comput. Model. Eng. Sci.* **2001**, *2*, 237–258.
23. Kim, M.; Yun, I. An efficient implementation of the generalized minimum residual algorithm with a new preconditioner for the boundary element method. *Eng. Anal. Bound. Elem.* **2011**, *35*, 1214–1224.
24. Mandel, J. On block diagonal and Schur complement preconditioning. *Numerische Mathematik* **1990**, *58*, 79–93.
25. ICNIRP. Guidelines for Limiting Exposure to Time-Varying Electric and Magnetic Fields (1 Hz - 100 kHz). *Health Phys.* **2010**, *99*, 818–836.